Icarus 212 (2011) 463–469

Contents lists available at ScienceDirect

Icarus

journal homepage: www.elsevier.com/locate/icarus

Laboratory studies on the sputtering contribution to the sodium atmospheres of Mercury and the Moon

Catherine A. Dukes *, Wen-Yen Chang, Marcelo Famá, Raúl A. Baragiola

Laboratory for Atomic and Space Physics, University of Virginia, 395 McCormick Road, Charlottesville, VA 22904, USA

ARTICLE INFO

Article history:
Received 7 September 2010
Revised 26 January 2011
Accepted 26 January 2011
Available online 1 February 2011

Keywords:
Mercury, Atmosphere
Moon, Surface
Solar wind
Spectroscopy

ABSTRACT

To ascertain the importance of sputtering by solar wind ions on the formation of a sodium exosphere around Mercury and the Moon, we have irradiated with 4 keV He ions, the Na bearing tectosilicates: albite, labradorite, and anorthoclase, as well as adsorbed Na layers deposited on albite and on olivine (a neosilicate that does not contain Na). Sodium at the surface and near surface (<40 Å) was quantified with X-ray photoelectron spectroscopy before and after each irradiation to determine the depletion cross section. We measured a cross section for sputtering of Na adsorbed on mineral surfaces, $\sigma_s \approx 1 \times 10^{-15}$ cm^2 atom^{-1}. In addition, mass spectrometric analyses of the sputtered flux show that a large fraction of the Na is sputtered as ions rather than as neutral atoms. These results have strong implications for modeling the sodium population within the mercurian and the lunar exospheres.

© 2011 Elsevier Inc. All rights reserved.

1. Introduction

The three recent Mercury flybys completed by the MErcury Surface, Space ENvironment, GEochemistry, and Ranging (MESSENGER) spacecraft have highlighted the importance of Na within the mercurian exosphere, where Na^+ was observed to be the dominant ionic species (Zurbuchen et al., 2008). Measurements of neutral sodium have indicated strong enhancement at high latitudes where magnetic field lines direct low energy (~1 keV amu^{-1}) protons and He ions from the solar wind ions to impact on the surface (McClintock et al., 2008, 2009; Vervack et al., 2010). This increased production of neutral sodium near the poles is thought to be dominated by ion sputtering of the planetary surface (Potter and Morgan, 1990) or desorption by solar photons enhanced by a proposed ion-induced diffusion of Na to the surface (Mura et al., 2009; Burger et al., 2010).

Understanding the exosphere of Mercury is of primary importance because it provides information on the planet's atomic surface composition, hinted at by the Mariner 10 mission and ground based measurements. By extrapolating from MESSENGER's atmospheric measurements, it becomes possible in principle to deduce the major surface sources and sinks for each atmospheric component, in particular sodium, as well as to constrain mechanisms involving thermal desorption and interactions between the surface and its space environment. These interactions include bombardment of the surface by photons, solar wind ions and electrons, as well as meteorites, and have been extensively modeled (see, e.g., Mangano et al., 2009; Mura et al., 2009; Burger et al., 2010).

Sodium has also been observed in the exosphere of the Moon (Potter and Morgan, 1985, 1988). Although alkali atoms are only a minor component of this atmosphere (Heiken et al., 1991), with average neutral atom densities of only ~70 sodium cm^{-3} and 15 potassium cm^{-3} near the surface (Potter and Morgan, 1988), they can be easily detected by their large resonance light scattering cross sections and provide a useful probe of the exosphere.

Observations of Mercury show that a significant amount of exospheric Na is suprathermal, with average kinetic energies equivalent to temperatures of several thousand degrees (Potter and Morgan, 1997; Killen et al., 1999), similar to that found for the Moon (Potter and Morgan, 1998). The energies are consistent with sputtering, photodesorption by solar UV, and meteoritic impact vaporization processes that eject alkalis present in the soil within silicate minerals or oxides into the exosphere. The ejected neutral Na supplied to the exosphere can be eventually photo-ionized and picked up by magnetic fields, contributing to Mercury's ion population.

A standard assumption has been that PSD (photon-stimulated desorption) by solar UV photons is the dominant source of Na in Mercury's exosphere (McGrath et al., 1986). Laboratory simulations conducted by Yakshinskiy and Madey (1999, 2000, 2004) found that light of wavelength shorter than 310 nm (>4 eV) desorbed Na from a layer of Na deposited onto SiO_2 and lunar basalt. That PSD can be the dominant source of sodium at the Moon was also inferred from the observation of sodium during a total lunar eclipse (Mendillo and Baumgardner, 1995), when the Moon was

* Corresponding author. Fax: +1 434 924 1353.
E-mail address: cdukes@virginia.edu (C.A. Dukes).

0019-1035/$ - see front matter © 2011 Elsevier Inc. All rights reserved.
doi:10.1016/j.icarus.2011.01.027

shielded from the solar wind, and during the passage of the Moon through the Earth's magnetotail (Potter et al., 2000; Sarantos et al., 2010).

However, the exospheric sodium is not spatially distributed around Mercury as expected from a PSD or thermal source (Potter and Morgan, 1990; Sprague et al., 1997; Potter et al., 1999). Rather, at times, Na is concentrated at northern or southern high latitudes and its distribution changes significantly over short time intervals. Killen et al. (2001) proposed that sputtering by solar wind particle precipitation at the magnetospheric cusp enhances the sodium exosphere at high latitudes. Whenever Mercury's magnetosphere is subjected to a southward interplanetary magnetic field, a larger portion of the surface is accessible to solar wind ions. The significance of this exospheric source has been modeled using uncertain theoretical values of sputtering yields. Experimental sputtering yields from reasonable analogs of Mercury's surface are required to improve current exospheric models. Sputtering experiment were done by Yakshinskiy and Madey (2004) using Na deposited on a lunar basalt thick section then irradiated by 3 keV Ar^+. However, these slow heavy ions are not representative of the solar wind and can remove deposited Na not only by sputtering, but by implantation deep in the material.

To elucidate the contribution of sputtering by solar wind ions to the atmospheres of Mercury and the Moon, we conducted laboratory simulations of solar wind interaction with planetary surfaces. We measured the sputtering of Na from minerals by 4 keV He^+ ions using X-ray photoelectron spectroscopy (XPS) and secondary ion mass spectroscopy (SIMS). Although our apparatus did not allow us to use a proton beam, the results for He^+ are important because the helium flux produces ~30% of the sputtering by the solar wind (Wurtz et al., 2010). TRIM calculations for 4 keV He^+ on stoichiometric albite suggest a sputtering yield ~5× larger than for 1 keV protons (Ziegler, 2008). In addition, our experimental results for He can be used to calibrate standard computer simulations for other ions.

Our results show clearly that the release of Na from a mineral surface strongly depends on the abundance of Na in the soil, the irradiation history, and that sodium ions are an important fraction of the sputtered ejecta.

2. Experimental methods

We investigated sputtering of sodium using a set of sodium-containing silicates and a set of Na-coated minerals. Using X-ray photoelectron spectroscopy, we quantified the decrease in the surface Na concentration as a function of irradiation fluence (ions cm^{-2}). In addition, we used secondary ion mass spectrometry to obtain the ionic composition of the sputtered flux.

Several terrestrial plagioclase feldspars were chosen for their relatively high Na content and mineralogical similarity to anorthosite, a ubiquitous lunar highland basalt: albite [$NaAlSi_3O_8$], labradorite [$(Na,Ca)Si_3O_8$], and anorthoclase [$(K,Na)AlSi_3O_8$]. In addition, olivine [$(Mg,Fe)_2SiO_4$], which contains no intrinsic Na, was used as a control. Samples were cleaned in an ultrasonic bath of methanol, and then rinsed with high purity (HPLC) water. One set of minerals was mounted directly, after cleaning, onto a copper sample platen and admitted to the vacuum chamber. A second set was pulverized in a clean, plastic bag, and powder grains <2 mm in size were fixed to the sample holder with microscopy-grade conductive carbon tape.

To measure the depletion cross section for vapor-deposited Na we evaporated, in vacuum, a fraction of a monolayer of Na onto the minerals, olivine or albite. These samples were sputter cleaned with 4 keV He^+ before evaporation to remove atmospheric contamination – primarily carbon. Sodium was evaporated from a small alkali metal dispenser from SEAS Getters and deposited for 30 min. XPS was used to measure the composition of the surface before and after sodium evaporation, and no more than a single monolayer was deposited. The temperature of the substrate was ~40 °C during deposition.

All of the irradiation experiments were conducted in an ultra-high vacuum (base pressure: $\sim 10^{-9}$ Torr) Physical Electronics 560 XPS/SAM system, equipped with a dual anode (Al/Mg) X-ray source mounted perpendicular to the double-pass, cylindrical-mirror electron energy analyzer (CMA). XPS is a quantitative surface analytical technique that uses mono-energetic X-rays (E_x = 1486.6 eV for Al–K$\alpha_{1,2}$) that penetrate the sample surface ejecting electrons of a characteristic binding energy (BE) with respect to the Fermi level. These photoelectrons have a kinetic energy in the spectrometer: $KE = E_x - BE - \Phi$, where Φ is the measured work function of the spectrometer. The signal is provided by those photoelectrons leaving the sample surface without energy loss, originating from a thin surface layer (20–40 Å thick on average, depending on the photoelectron energy). Quantitative information is obtained by incorporating the instrument sensitivity for each elemental transition, which has an accuracy of ~15%. The CMA was operated at an energy resolution of 3.2 eV to provide high sensitivity, ensuring that all the surface constituents on each mineral were identified to the <1% level. Data were taken using primarily Al (K$\alpha_{1,2}$) X-rays to minimize the overlap of Auger and photoelectron spectra.

We conducted irradiations using a 4 keV He ion beam from a differentially pumped electron-impact type ion source. The ion beam was rastered uniformly over the sample and across the analysis area. The average angle of incidence with respect to the surface normal was either 53° or 0°, depending on the particular experiment. We note that local incidence angles vary on powder samples. A movable Faraday cup with a 0.54 mm diameter aperture, mounted adjacent to the sample, was used to measure ion beam current density before and after irradiations. To neutralize differential electrostatic charging across the mineral surface we used low energy electrons from a flood gun without charge bias. A sample manipulator allowed samples to be rotated between irradiation and analysis positions, as well as translated for Na vapor deposition without removal from the analysis chamber.

3. Results

A representative XPS photoelectron spectrum for albite shows Na, Si, Al, O, and C on the surface along with small amounts of Ca (Fig. 1), due to random and non-random substitutions for Na in the interstitial regions between SiO_4 and AlO_4 tetrahedra (Klein and Hurlbut, 1977). Cation substitutions are required to provide charge neutralization where Si^{4+} is substituted for Al^{3+} or vice versa. Carbon is a normal impurity in terrestrial igneous rock and is often a remnant of carbon dioxide or carbonate, acquired during mineral formation. The signal may also include a small amount of adventitious carbon incompletely removed by ion bombardment prior to Na deposition.

3.1. Removal of adsorbed and intrinsic Na by ion irradiation

We acquired XPS spectra vs. ion fluence and measured the area of the Na-1s photoelectron peak, as well as Si-2s, Al-2p, O-1s, Ca-2p, and C-1s, and used them to obtain the Na surface concentration relative to Si, through sensitivity factors. Samples of terrestrial albite, anorthoclase and labradorite (Fig. 2) were studied to measure the surface depletion of intrinsic sodium (bound within the mineral structure) under ion irradiation. In all cases, the Na concentration follows a similar exponential decay, with a depletion cross section (decay constant) of 1.4×10^{-17} cm^2 $atom^{-1}$ for albite,

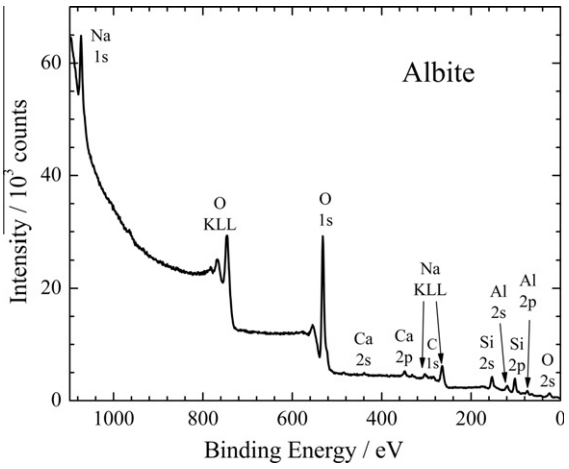

Fig. 1. Representative XPS spectrum of albite obtained with Al–K X-rays. The photoelectron lines are identified by the element and the energy level of the ejected electron. The KLL structures are due to the Auger process following the creation of a K-shell hole. The Na-1s photoelectron peak at a binding energy of ~1072 eV was used to determine the amount of sodium present on the mineral surface.

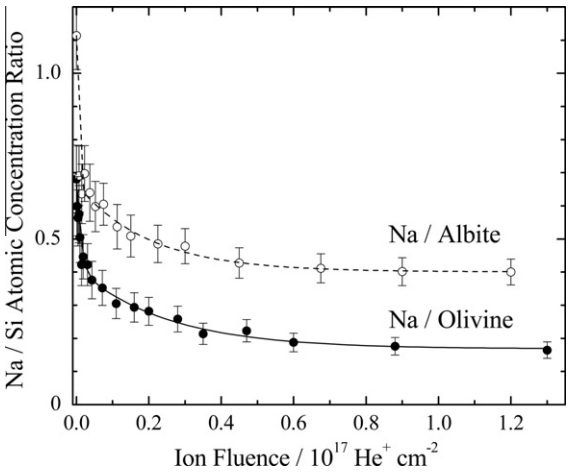

Fig. 3. Na:Si concentration on a sub-monolayer of Na deposited on ion-roughened albite rock and olivine powder vs. 4 keV He^+ fluence. The Na:Si ratios are fit by a double exponential function plus a constant term (see text) with decay constants of 9×10^{-16} cm^2 atom^{-1} and ~4.5×10^{-17} cm^2 atom^{-1}.

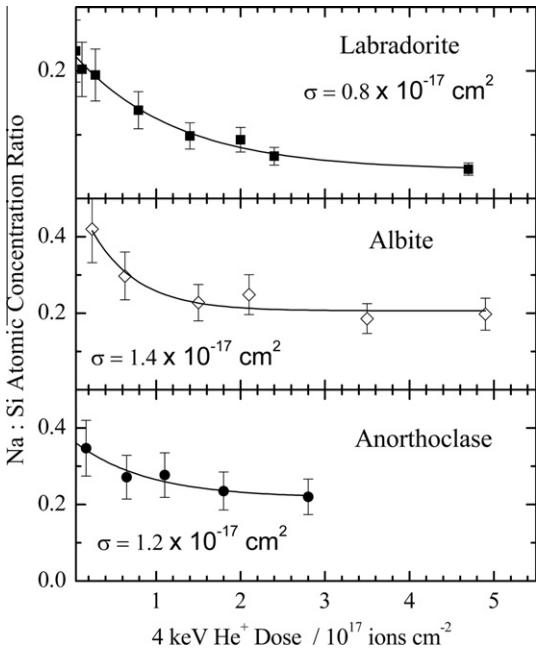

Fig. 2. Decrease in the surface concentration of Na relative to Si in cleaved minerals vs. fluence of 4 keV He^+. The lines are exponential fits to the data (see text) with decay constants of 0.8, 1.4, and 1.2×10^{-17} cm^2 ion^{-1} for labradorite, albite, and anorthoclase, respectively.

1.2×10^{-17} cm^2 atom^{-1} in anorthoclase, and 0.8×10^{-17} cm^2 atom^{-1} for labradorite.

Since sodium released from the surface of Mercury and the Moon can re-deposit as a coating on different mineral surfaces by the action of gravity, we then measured the depletion of sub-monolayer deposits of sodium on albite and olivine (powder or cleaved rock). Fig. 3 shows the decrease of the sodium surface concentration with fluence. The results are strikingly different from those in the uncoated samples of Fig. 2. Instead of a single exponential decay, the results can be fit to a double exponential decay. The initial decay is about two orders of magnitude faster than that of the intrinsic Na, with a depletion cross section of 9×10^{-16} cm^2 atom^{-1}. The second exponential decay is similar to that of the Na-containing minerals, with a decay constant of ~4.5×10^{-17} cm^2 atom^{-1} for both olivine and albite samples.

Because surface binding of adsorbed atoms is weaker than that of atoms embedded in the bulk, we assign the first decay to depletion of surface Na. As will be shown later, the second decay is given by Na in the bulk being depleted by ion impact. The equilibrium concentration at high fluences is the original bulk concentration plus that resulting from diffusion during sodium deposition, as well as from deeper within the bulk – a process discussed in detail later.

The depletion of intrinsic sodium due to irradiation is reversed with time by diffusion. For instance, at room temperature the Na:Si ratio in albite decays from 0.33 to 0.17 after irradiation but then recovers after sitting 15, 25, and 40 h in vacuum to 0.23, 0.30 and 0.31 respectively. The diffusion rate, which is expected to increase at higher temperatures, is important for understanding the generation of alkali exospheres (Killen and Morgan, 1993).

3.2. Sputtering of neutral and ionized sodium

Secondary ion mass spectrometry (SIMS) is a highly sensitive technique for studying surfaces by analysis of sputtered ions. Elphic et al. (1991) have shown that 1.5 keV H^+ and 4 keV He^+ irradiation of lunar soil simulants provides useful information of surface composition. We used SIMS to study Na^+ emission during irradiation with 4 keV He^+ utilizing an Advanced R&D SIMS system comprised of a Balzers 311 quadrupole ion mass spectrometer with a front-end energy filter. Fig. 4 shows a typical SIMS mass spectrum for Na-depleted albite after high fluence 4 keV He irradiation. The spectrum displays an array of albite's constituents: Na^+, Ca^+ (Ca^{++}), Al^+, Si^+, O^+, as well as a molecular species: NaO^+. Mass 39 amu is assigned to NaO, rather than K^+, since no potassium was seen with XPS. No other molecular species such as $NaOH^+$, NaO_2^+, $Na(OH)_2^+$, or SiO^+, are observed within the sensitivity of the instrument. Although oxygen is a major constituent of bulk albite, the positive secondary ion production of O^+ is very low (<1% Si^+) as a result of 4 keV He^+ bombardment, which depletes the surface of oxygen, and the relatively high ionization potential of oxygen, which favors neutralization.

To compare the Na depletion of the albite surface as seen by XPS with the Na actually sputtered from the surface observed with SIMS, we used pristine albite samples *not* coated with Na. Fig. 5 shows the fluence dependence of the signal of desorbed Na^+ measured with SIMS, a technique sensitive mainly to the outermost atomic layer, and the surface Na:Si concentration ratio measured

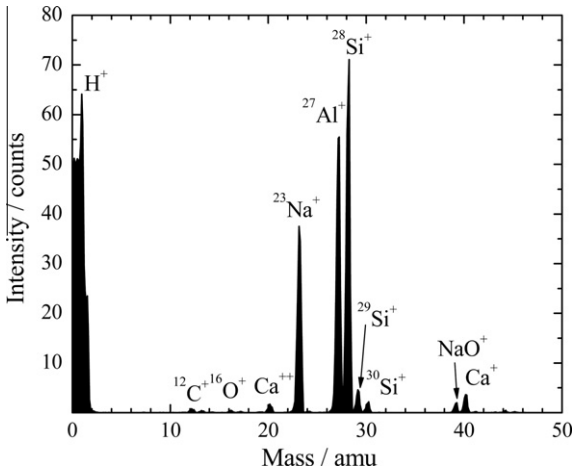

Fig. 4. SIMS spectrum induced by 4 keV He^+ on albite that has been partially depleted of Na by high fluence irradiation. The ions ejected from the mineral surface are Na^+, Al^+, Si^+ (all isotopes in proportion), Ca^+ (and Ca^{++}), O^+, C^+, as well as one Na-bearing molecular ion: NaO^+.

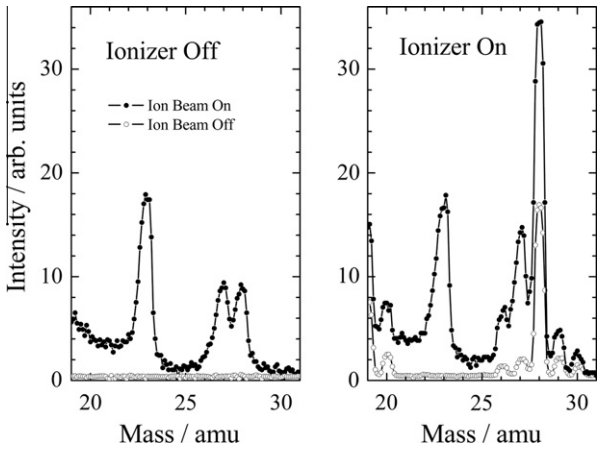

Fig. 6. Mass spectra measured with a quadrupole mass spectrometer directed at the sample, for 4 keV He^+ on albite. (Left panel) No post-ionization, solid dots show sputtered Na^+, Si^+, and Al^+ with the ion beam on, while the open dots show only background with the ion beam off. (Right panel) Same as left panel but with post-ionization in the mass spectrometer. With the ion beam on the sample, the signal is from sputtered ions and sputtered atoms, as well as background gas atoms.

with XPS. We observe the ejected Na intensity falls with ion fluence in an identical fashion to XPS, with a depletion decay constant of 3.9×10^{-17} cm^2. This value, for a smooth surface, is a factor of ~3 larger than observed for a rough surface (Fig. 2) where a fraction of the sputtered flux is captured by adjacent grains. The fact that the decay of the surface concentration is the same as that of the sputtered ion flux demonstrates that the Na^+ SIMS signal (originating from a depth <0.5 nm) is proportional to the surface Na concentration seen by XPS, which has an information depth of about 4 nm. The depletion time constant should not be confused with a sputtering cross section since, as will be shown in the discussion, it is related to *differential* sputtering with respect to other species, and to redistribution of Na in the bulk.

To investigate the charge and mass composition of the sputtered flux (from albite) we used a Stanford Research Systems RGA100 quadrupole mass spectrometer. This instrument can be operated with the ionizer on, measuring neutrals and ions, or off, detecting only ions. Fig. 6 shows mass spectra of species ejected from the surface of albite that has *not* been partially depleted of Na by high fluence irradiation (in contrast to Fig. 4). The spectra were taken both with (Fig. 6 right panel) and without (Fig. 6 left panel) post-ionization of the sputtered flux by electrons in the ion source of the mass spectrometer. The secondary ion spectra clearly shows sodium (mass 23), suggesting that a significant fraction of sputtered Na is removed as an ion, as well as Al^+ and Si^+, similar to Fig. 4. No Na^+ is ejected without the ion beam, and the Na^+:(Na^0 + Na^+) ratio can be roughly gauged by comparing the peak heights with the RGA filament off to that with the RGA filament on. Additional ionization in the mass spectrometer does not increase the Na signal, but that of other mass peaks derived from the vacuum chamber background gases. Small discrepancies between Figs. 4 and 6 (left panel) are attributed to sample variation and partial Na depletion of the albite shown in Fig. 4. The sensitivity of SIMS depends on many parameters, such as the ionization state of the element in the sample, projectile and sputtered ion energies, and instrumental factors. The relative sensitivity of our mass spectrometer for neutrals and ions are of the same order, as gauged by comparison of the relative XPS and SIMS intensities. The ratios of SIMS signals, Na:Si and Na:Al are the same as those for XPS, within ~30%. This confirms the study by Elphic et al. (1991) which demonstrates that the fraction of Na, Al, and Si atoms sputtered as positive ions are similar in magnitude and can be used as a good estimate of the surface composition for silicates, and highlights the value of SIMS for the analysis of minerals.

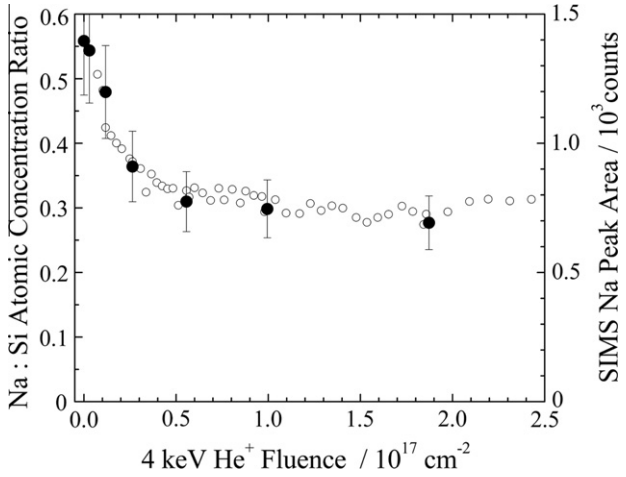

Fig. 5. Na:Si concentration ratio (XPS signal) from a smooth albite surface vs. 4 keV He^+ irradiation fluence (filled circles). SIMS signal of Na^+ sputtered from the same surface (open circles). A fit to a single exponential decay gives a depletion cross section of 3.9×10^{-17} cm^2 $atom^{-1}$.

4. Discussion

4.1. Preferential sputtering

Changes in surface concentration due to ion impact are ascribed to a species-dependent phenomena occurring in the cascade of atomic collisions initiated by the impinging ion. For 4 keV He, about half the collisions are electronically elastic, where momentum and energy is exchanged between the atoms. Since the elastic energy transfer depends on the mass of the colliders, the energy deposition into atomic motion is unevenly distributed among the different types of atoms in the solid (e.g., energy transfer increases as He collides with O, Na, and Si). The collision cascade can produce sputtering when it reaches the surface. The depth of origin of sputtered atom, 2–3 layers (Betz and Wehner, 1983), is somewhat larger for light than heavy atoms due to their lower energy loss in collisions. Therefore, the sputtering yield of a particular atom is, to first order, proportional to its surface concentration and the

collisional energy deposited at the topmost 1–3 atomic layers of the solid, and inversely proportional to its surface binding energy. These species-dependent effects lead to preferential sputtering (Shimizu, 1987).

Sputtering can be understood starting with the analytical theory of Sigmund (1969), which has great predictive power. The limitation of the theory to describe only simple solids can be removed, in the most part, by the SRIM implementation of Biersack's TRIM Monte Carlo program (Ziegler et al., 2008). This model is based on the same physical picture as Sigmund's theory (e.g., binary collisions in random solids) but can use arbitrary atomic composition vs. depth in the material and can calculate deposited energies taking into account the complexity of multi-component materials. We computed a million histories of 4 keV He at normal incidence on a target with a homogeneous composition of albite, using the default binding energy values provided by SRIM. We obtained a He reflection probability of 0.064, most probable and maximum penetration depths of 40 and 100 nm, and an average sputtering yield of 0.30 atoms ion^{-1} (0.037 for Na). This value is in close agreement with the measured experimental value for SiO_2, which implies the removal of ~0.4 nm of material per 10^{16} He cm^{-2}. Uncertainties in the interatomic (interionic) potentials and in the surface and bulk binding energies of the different atoms make the simulation uncertain by an estimated 40%. Monte Carlos TRIM calculations indicate that for 1 keV H, the sputtering yields are ~5.5 times smaller than those for 4 keV He.

The simulation gives O and Na sputtering yields of 0.20 and 0.037, respectively. Normalized to the atomic fraction, these sputtering yields are 0.37 and 0.48, higher than the mean sputtering yield of 0.30, indicating the preferential sputtering of Na and O. This is expected based on numerous studies that show that oxygen is preferentially sputtered from glasses, metal oxides and minerals (Kelly, 1987; Betz and Wehner, 1983; Malherbe et al., 1986; Hochella et al., 1988). It leads to a chemical reduction of the lunar regolith (Johnson and Baragiola, 1991) and the formation of metallic iron in olivine (Dukes et al., 1999; Loeffler et al., 2009). Preferential sputtering of Na and other alkalis has also been observed previously for many glasses and metal oxides (see, e.g., Battaglin et al., 1986; Torrisi et al., 1988; Arnold, 1989).

We note that TRIM does not take into account surface morphology, which influences sputtering because of shadowing and re-deposition. Unlike the planar surface assumed by TRIM, the regoliths of the Moon and Mercury are grainy and porous due to meteoritic impacts over millions or billions of years (Hapke, 1986). A comparison of Figs. 2 and 5 shows a reduction of 64% in the depletion of Na from granular vs. flat surfaces of albite. This is in good agreement with recent experimental studies by Loeffler et al. (2009) that show a reduction of ~67% for a carbon surface layer on olivine powder.

4.2. Effects of accumulated fluence

As a result of continuous irradiation, the composition of multi-component materials and their depth dependence, change concurrently with fluence. Atomic redistribution or mixing by collisional displacements (including preferential sputtering) and diffusion enhanced by the vacancies created in the collisions create a surficial region called the "altered layer" with a composition different from that of the bulk up to depths close to the maximum range of the projectiles (Liau et al., 1978; Varga and Taglauer, 1984; Sigmund and Lam, 1993). For insulators, there is an additional, little-known effect of ionic motion due to internal electric fields resulting from ionizing collisions. For instance, a positive surface charge resulting from electron ejection and from the implantation of the ion charge provide an electric field that can induce migration of Na^+ ions inside the solid, towards or away from the surface depending on the location of the charge. In this series of experiments, where any excess charged was neutralized by the flood of thermal electrons, the effect of residual electric fields is likely unimportant (Magee and Harrington, 1978).

By itself, the preferential sputtering of Na would lead to a surface depletion of this element, limited to the depth of origin of sputtered atoms (2–3 monolayers). However, the projectiles also accelerate diffusion of Na within the ion range, due to the vacancies they generate. Excess Na is trapped at the top monolayer by Gibbsian segregation (Sigmund and Lam, 1993), which enhances the Na concentration at the albite surface and accelerates the sputtering of Na. This surface segregation occurs at the expense of a reduced concentration of Na below the surface. In addition, the collision cascade relocates atoms throughout the ion range region (collisional mixing), leading to the smearing of concentration gradients. Therefore, the complex nature of the different processes outlined here implies that the depletion cross section cannot be equated to a sputtering cross section.

4.3. Sputtering of adsorbed sodium

The sputtering of a monolayer of foreign atoms on surfaces has been investigated extensively (Taglauer, 1990). The initial decay of the Na surface density N (atoms cm^{-2}) F is given by

$$N(F) = N_s(0)\exp(-\sigma F) + N_b \quad (1)$$

where σ is a depletion cross section, N_s the density of the Na monolayer coating and N_b the Na density produced by its bulk Na concentration. The cross section is related to the sputtering yield by $Y = \sigma_d N(F)$, and is a better quantity for an atomistic description. The measured desorption cross section for adsorbed Na, 1×10^{-15} cm^2 is about 4 times larger than 2.6×10^{-16} cm^2, which we simulated using TRIM.

Depletion can result, not only from sputtering but also from preferential recoil implantation of one component into the bulk due to small impact parameter collisions between the ion and a surface atom. This process has been observed for heavier projectiles (Morita, 1993) but is unimportant in the case of 4 keV He projectiles. Due to the small He mass and nuclear potential, the cross section for energy transfer greater than the 2 eV to a Na atom, required for its implantation into the bulk, is only 5×10^{-17} cm^2, as calculated with the ZBL potential (Ziegler et al., 1985). This cross section is only ~2% of the total Na depletion cross section found in our experiments, making recoil implantation of Na negligible in collisions of light projectiles, such as H and He in the solar wind. The low probability of recoil implantation implies that the amount of Na depleted by this mechanism is only 2% of the deposited layer, or ~10^{13} atoms cm^{-2}. TRIM shows that the recoil distribution falls exponentially in depth with a decay constant of ~1 nm, giving an average bulk concentration of ~10^{20} Na cm^{-3}, or ~0.3 at.%, which is at the background level for the XPS technique. Thus, the Na surface concentration observed in olivine, which does not contain intrinsic Na, after the overlayer is removed is not due to recoil implantation of the surface layer, but a result of in-diffusion of Na during vapor deposition, when the surface is heated tens of degrees above room temperature by thermal radiation from the evaporation source.

4.4. Fraction of Na^+ in the sputtered flux

Our experiments show that the fraction of ions in the Na sputtered flux is close to unity. This result is consistent with previous experiments on other ionic compounds, which have shown that the sputtered flux from such solids has a large percentage of ions. Benninghoven and Mueller (1972) reported sputtered ion yields for oxides close to the total sputtering yields. Steinbrüchel and Gruen

(1980, 1981) measured ion fractions of 0.4–0.8 from metal oxides. Sputtering measurements on minerals by Andersen and Hinthorne (1972) were interpreted by the authors using a thermal spike model that predicts ion fractions close to 1 for Na, Mg, Al and Si. The authors validated the predictive value of this model by applying it to the SIMS analysis of lunar rocks which gave compositions in agreement with those obtained by other methods. Similar conclusions were reached by Elphic et al. (1991) from their SIMS measurements of lunar soil simulants induced by light ions.

A high ion/neutral ratio of sodium from a planetary surface is important because the trajectory of Na^+ will be affected not only by gravity, as happens with Na^0, but also by magnetic and electrical fields in the planetary environment.

5. Conclusions

The major results of this study are: the absolute value of sputtering cross section for adsorbed Na ($\sigma_s \approx 1 \times 10^{-15}$ cm^2 atom^{-1}), the predominance of ions in the Na sputter flux and the similar results for different Na-bearing minerals. The sputtering cross section for incorporated Na, though likely smaller than that for adsorbed Na, cannot be inferred simply from the decay constant, since this constant is also a function of the Na concentration in the bulk and of near-surface, radiation-induced diffusion. Even though we report results only for Na, it is important to note that all elements are ejected, and, therefore sputtering will contribute to the abundance of the different species present in exospheres of the Moon or Mercury. It is likely that a number of proposed ejection processes: sputtering, photodesorption and micrometeorite bombardment are important in exospheric generation depending on the relative flux of impactors. Unlike photodesorption, which is solely a surface process, sputtering and meteoritic impact can remove Na even from beneath the surface. Sodium can then redeposit as an adsorbed layer on the surface, where it can be removed more easily by another event, including photodesorption. The cycle of desorption and re-deposition is interrupted by the removal of Na from the atmosphere through different escape processes. The high fraction of Na, Al and Si ions in the sputtered flux should be considered in models describing the relation between the surface and the exosphere.

Acknowledgments

This research was supported by the NASA Cosmochemistry (NNX08AG72G) and Planetary Atmospheres program and by NSF Astronomy (AST0807830). We acknowledge productive discussions with T.E. Madey and A. Sprague.

References

Andersen, C.A., Hinthorne, J.R., 1972. Ion microprobe mass analyzer. Science 175, 853–860.
Arnold, G.W., 1989. Light element redistribution and property changes in insulators due to ion bombardment and chemical processing. Nucl. Instrum. Methods Phys. Res. B39, 708–715.
Battaglin, G., Boscoletto, A., Della Mea, G., De Marchi, G., 1986. Heavy ion irradiation of glasses: Enhanced diffusion and preferential sputtering of alkali elements. Rad. Eff. 98, 101–108.
Benninghoven, A., Mueller, A., 1972. Secondary ion yields near 1 for some chemical compounds. Phys. Lett. 40A, 169–170.
Betz, G., Wehner, G.K., 1983. Sputtering of multicomponent materials. In: Behrisch, R. (Ed.), Sputtering by particle bombardment II, Top. Appl. Phys., 52. Springer, New York, pp. 11–90.
Burger, M.H. et al., 2010. Monte Carlo modeling of sodium in Mercury's exosphere during the first two MESSENGER flybys. Icarus 209, 63–74.
Dukes, C.A., Baragiola, R.A., McFadden, L.A., 1999. Surface modification of olivine by H^+ and He^+ bombardment. J. Geophys. Res. – Planets 104, 1865–1872.
Elphic, R.C. et al., 1991. Lunar surface composition and solar wind-induced secondary ion mass spectrometry. Geophys. Res. Lett. 18, 2165–2168.
Hapke, B., 1986. On the sputter alteration of regoliths of outer Solar System bodies. Icarus 66, 270–279.
Heiken, G.H., Vaniman, D.T., French, B.M., 1991. Lunar Sourcebook: A User's Guide to the Moon. Cambridge Univ. Press, Cambridge (Chapters 5 and 8).
Hochella, M.F., Lindsay, J.R., Mossotti, V.G., Eggleston, C.M., 1988. Sputter depth profiling in mineral-surface analysis. Am. Mineral. 73, 1449–1456.
Johnson, R.E., Baragiola, R.A., 1991. Lunar surface: Sputtering and secondary ion mass spectrometry. J. Geophys. Res. 18, 2169–2172.
Kelly, R., 1987. The sputtering of insulators. In: Mazzoldi, P., Arnold, G.W. (Eds.), Ion Beam Modification of Insulators. Elsevier, Amsterdam (Chapter 2).
Killen, R.M., Morgan, T.H., 1993. Diffusion of Na and K in the uppermost regolith of Mercury. J. Geophys. Res. 98 (E23), 23589–23601.
Killen, R.M., Potter, A.E., Fitzsimmons, A., Morgan, T.H., 1999. Sodium D_2 line profiles: Clues to the temperature structure of Mercury's exosphere. Planet. Space Sci. 47, 1449–1458.
Killen, R.M. et al., 2001. Evidence for space weather at Mercury. J. Geophys. Res. 106, 20509–20520.
Klein, C., Hurlbut Jr., C., 1977. Manual of Mineralogy. John Wiley and Sons, New York. pp. 541–543.
Liau, Z.L., Mayer, J.W., Brown, W.L., Poate, J.M., 1978. Sputtering of PtSi. J. Appl. Phys. 49, 5295–5305.
Loeffler, M.J., Dukes, C.A., Baragiola, R.A., 2009. Irradiation of olivine by 4 keV He^+: Simulation of space weathering by the solar wind. J. Geophys. Res. 114, E0303–E0316.
Magee, C.W., Harrington, W.L., 1978. Depth profiling of sodium in SiO films by secondary ion mass spectrometry. Appl. Phys. Lett. 33, 193–196.
Malherbe, J.B., Hofmann, S., Sanz, J.M., 1986. Preferential sputtering of oxides: A comparison of model predictions with experimental data. Appl. Surf. Sci. 27, 355–365.
Mangano, V. et al., 2009. Detection of a southern peak in Mercury's sodium exosphere with the TNG in 2005. Icarus 201 (2), 424–431.
McClintock, W.E. et al., 2008. Spectroscopic observations of Mercury's surface reflectance during MESSENGER's first Mercury flyby. Science 321 (5885), 62–65.
McClintock, W.E. et al., 2009. MESSENGER observations of Mercury's exosphere: Detection of magnesium and distribution of constituents. Science 324, 610–613.
McGrath, M.A., Johnson, R.E., Lanzerotti, L.J., 1986. Sputtering of sodium on the planet Mercury. Nature 323, 694–696.
Mendillo, M., Baumgardner, J., 1995. Constraints on the origin of Moon's atmosphere from observations during a lunar eclipse. Nature 377, 404–406.
Morita, K., 1993. Recoil implantation effects in ion impact desorption of monolayer adsorbates on solid surfaces. Nucl. Instrum. Methods Phys. Res. B78, 171–180.
Mura, A. et al., 2009. The sodium exosphere of Mercury: Comparison between observations during Mercury's transit and model results. Icarus 200, 1–11.
Potter, A.E., Morgan, T.H., 1985. Discovery of Na in the atmosphere of Mercury. Science 229, 651–653.
Potter, A.E., Morgan, T.H., 1988. Discovery of sodium and potassium vapor in the atmosphere of the Moon. Science 241, 675–680.
Potter, A.E., Morgan, T.H., 1990. Evidence for magnetospheric effects on the sodium atmosphere of Mercury. Science 248, 835–838.
Potter, A.E., Morgan, T.H., 1997. Evidence for suprathermal sodium on Mercury. Adv. Space Res. 19, 1571–1576.
Potter, A.E., Morgan, T.H., 1998. Coronagraphic observations of the lunar exosphere near the lunar surface. J. Geophys. Res. 103 E, 3581–3586.
Potter, A.E., Killen, R.M., Morgan, T.H., 1999. Rapid changes in the sodium exosphere of Mercury. Planet. Space Sci. 47, 1441–1448.
Potter, A.E., Killen, R.M., Morgan, T.H., 2000. Variation of lunar sodium during passage of the Moon through the Earth's magnetotail. J. Geophys. Res. 105, 15073–15084.
Sarantos, M., Killen, R.M., Sharma, A.S., Slavin, J.A., 2010. Sources of sodium in the lunar exosphere: Modeling using ground-based observations and spacecraft data of the plasma. Icarus 205, 364–374.
Shimizu, R., 1987. Preferential sputtering. Nucl. Instrum. Methods Phys. Res. B18, 486–489.
Sigmund, P., 1969. Theory of sputtering. I. Sputtering yield of amorphous and polycrystalline targets. Phys. Rev. 184, 383–416.
Sigmund, P., Lam, N.Q., 1993. Alloy and isotope sputtering. Mat. Dys. Medd. Dan. Vid. Selsk. 43, 255–349.
Sprague, A.L. et al., 1997. Distribution and abundance of sodium in Mercury's atmosphere, 1985–1988. Icarus 129, 506–527.
Steinbrüchel, C., Gruen, D.M., 1980. Absolute measurements of sputtered ion fractions using matrix isolation spectroscopy. Surf. Sci. 93, 209–299.
Steinbrüchel, C., Gruen, D.M., 1981. Measurement of neutral and ion sputtering yields by matrix isolation spectroscopy. J. Vac. Sci. Technol. 18, 235–237.
Taglauer, E., 1990. Surface cleaning using sputtering. Appl. Phys. A 51, 238–251.
Torrisi, A., Marletta, G., Licciardello, A., Puglisi, O., 1988. Na-surface segregation and oxygen depletion in particle bombardment of alkaline glasses. Nucl. Instrum. Methods Phys. Res. B32, 283–287.
Varga, P., Taglauer, E., 1984. Depth profiling of the altered layer in Ta_2O_5 produced by sputtering with He ions. Nucl. Instrum. Methods Phys. Res. B2, 800–803.
Vervack Jr., R.J. et al., 2010. Mercury's complex exosphere: Results from MESSENGER's third flyby. Science 329, 672–675.
Wurtz, P. et al., 2010. Self-consistent modeling of Mercury's exosphere by sputtering, micro-meteorite impact and photon-stimulated desorption. Planet. Space Sci. 58, 1599–1616.

Yakshinskiy, B.V., Madey, T.E., 1999. Photon-stimulated desorption as a substantial source of sodium in the lunar atmosphere. Nature 400, 642–644.
Yakshinskiy, B.V., Madey, T.E., 2000. Desorption induced by electronic transitions of Na from SiO_2: Relevance to tenuous planetary atmospheres. Surf. Sci. 451, 160–165.
Yakshinskiy, B.V., Madey, T.E., 2004. Photon-stimulated desorption of Na from lunar sample: Temperature-dependent effects. Icarus 168, 53–59.
Ziegler J.F., Biersack, J.P., Littmark, U., 1985. In: Ziegler, J.F. (Ed.), The Stopping and Range of Ions in Solids. Pergamon, New York (Chapter 2).
Ziegler, J.F., Biersack, J.P., Ziegler, M.D., 2008. The Stopping and Range of Ions in Matter. SRIM Co.
Zurbuchen, T.H. et al., 2008. MESSENGER observations of the composition of Mercury's ionized exosphere and plasma environment. Science 321, 90–92.